High-Throughput Multiplexed Infrared Spectroscopy of Ion Mobility-Separated Species Using Hadamard Transform

Vasyl Yatsyna,* Ali H. Abikhodr, Ahmed Ben Faleh, Stephan Warnke, and Thomas R. Rizzo

Cite This: *Anal. Chem.* 2022, 94, 2912−2917

Read Online

ACCESS | Metrics & More | Article Recommendations | SI Supporting Information

ABSTRACT: Coupling vibrational ion spectroscopy with high-resolution ion mobility separation offers a promising approach for detailed analysis of biomolecules in the gas phase. Improvements in the ion mobility technology have made it possible to separate isomers with minor structural differences, and their interrogation with a tunable infrared laser provides vibrational fingerprints for unambiguous database-enabled identification. Nevertheless, wide analytical application of this technique requires high-throughput approaches for acquisition of vibrational spectra of all species present in complex mixtures. In this work, we present a novel multiplexed approach and demonstrate its utility for cryogenic ion spectroscopy of peptides and glycans in mixtures. Since the method is based on Hadamard transform multiplexing, it yields infrared spectra with an increased signal-to-noise ratio compared to a conventional signal averaging approach.
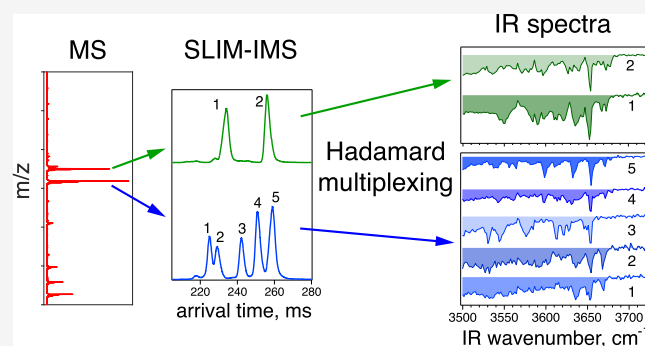
INTRODUCTION

Separation and identification of isomers are long-standing problems in analytical chemistry. They are particularly crucial in the fields of glycomics,[1−3] metabolomics,[4,5] and lipidomics,[6,7] where the high isomeric complexity of samples poses a significant analytical challenge. For example, glycans, also known as oligosaccharides or carbohydrates, are difficult to analyze due to their complex stereochemistry and the possibility of branched structures.[8] Likewise, many important metabolite molecules are isobaric or isomeric and difficult to identify.[5]

While mass spectrometry (MS) offers rapid analysis with extremely high sensitivity,[9] it cannot easily distinguish between isomers, and hence it is often combined with orthogonal separation techniques, such as liquid chromatography (LC),[2,4,10] capillary electrophoresis,[11] or gas chromatography.[12] Even though these hybrid techniques can separate many isomeric structures, the addition of an orthogonal separation method often extends the analysis time, which in the case of LC−MS can take more than an hour for a single separation procedure. Ion mobility spectrometry (IMS),[13−15] on the other hand, can separate isomers on a millisecond timescale and is easily coupled to MS, showing great promise for high-throughput analysis of complex isomeric mixtures. Recent developments in the high-resolution IMS technology such as structures for lossless ion manipulation (SLIM)[16,17] and cyclic IMS[18] make these techniques particularly well suited to isomer separation. Nevertheless, it remains challenging to assign unambiguously isomeric species in complex mixtures following high-resolution IMS separation, either using their collisional

cross sections (CCSs)[19−22] or tandem MS.[23−25] Recently, several research groups have applied infrared (IR) spectroscopy to distinguish isomeric ions, either at room temperature using IR multiple photon dissociation spectroscopy (IRMPD)[26−30] or under cryogenic conditions using messenger-tagging spectroscopy[31] or helium nanodroplet spectroscopy.[32−34] We have recently demonstrated that a combination of cryogenic IR spectroscopy with ultrahigh-resolution IMS offers an unambiguous identification of isomers with the subtlest of structural differences.[35−41] For instance, using this approach, glycan reducing-end anomers can be separated and distinguished by their cryogenic IR spectra.[35,36,38] The power of this technique stems from the fact that the vibrational spectrum is an intrinsic property of a molecule, which can be stored in a database, reproduced across laboratories, and can serve as a fingerprint for molecular identification. While adding a spectroscopic dimension to IMS−MS does increase the sample analysis time, we have recently developed a scheme in which IR fingerprints of multiple, mobility-separated species can be obtained in less than a minute.[42] Nevertheless, fast spectroscopic analysis of all species in a complex mixture still presents a challenge.

To address this issue further, we present here a novel multiplexed spectroscopic technique based on Hadamard transform that can be used to acquire simultaneously the IR spectra of all species present in a mixture in a single laser scan. This approach could be easily implemented on any IMS−MS instrument equipped with ion trapping and laser irradiation. Moreover, it is particularly well-suited for spectroscopic studies of complex mixtures with a broad range of ion mobilities. We demonstrate the method by recording the cryogenic IR spectra of all species separated by SLIM−IMS for several peptide and glycan mixtures and show that the spectral signal-to-noise ratio (SNR) increases in agreement with the theoretical multiplex advantage.

■ EXPERIMENTAL METHODS

Apparatus. Figure 1 shows a schematic representation of the home-built instrument that we used in this work, which has
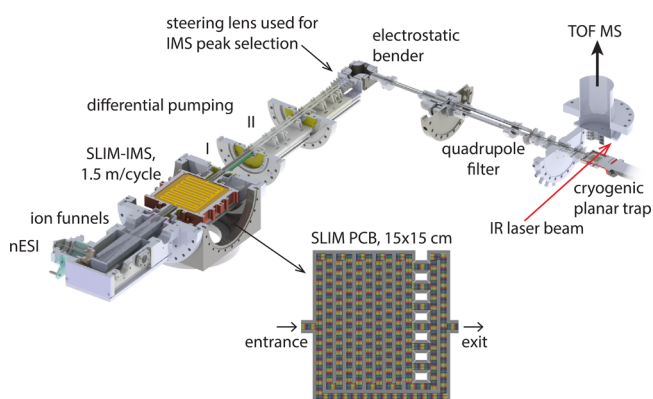

Figure 1. Overview of the experimental setup employed in this work. The figure is adapted with permission from ref 36. Copyright 2022 American Chemical Society.

been described previously.[36,43] It combines ultrahigh-resolution SLIM−IMS with cryogenic ion spectroscopy and time-of-flight (TOF) MS. In brief, ions produced by nanoelectrospray are introduced into the instrument through a heated stainless-steel capillary (170 °C) and accumulated in a dual-stage ion funnel assembly (MassTech), which we use as a trap. Short, intense ion packets (150 μs duration) are then released into a compact SLIM ion mobility device (15 × 15 cm) filled with helium at 3 mbar, where molecules are separated according to their shape (i.e., their rotationally averaged CCS). The SLIM−IMS device[43] was designed following the work of Smith and co-workers[16,17] and offers a single-cycle 1.5 m serpentine path for mobility separation. Extended path lengths are obtained by allowing the ions to undergo multiple cycles.[36,44] Following SLIM−IMS separation, mobility-selected ions are guided through differential pumping stages, an electrostatic bender, and a quadrupole before entering a cryogenic planar trap maintained at a temperature of 40 K. A short intense gas pulse (He/N_2 mixture, 9:1 ratio) is introduced shortly before arrival of the ions to trap them, cool them, and tag them with nitrogen in preparation for messenger-tagging spectroscopy. Subsequently, the cold tagged ions are irradiated with a tunable continuous-wave mid-IR laser (IPG Photonics) and mass analyzed using a reflectron-type TOF mass spectrometer. When the laser frequency is resonant with a vibrational transition of the tagged molecule, it absorbs an IR photon, which leads to intramolecular vibrational energy redistribution and dissociation of the nitrogen tag(s). Plotting the ratio between the tagged and total ion signals of the same species as a function of the laser wavenumber produces highly resolved IR spectra that can serve as fingerprints for molecular identification. Typical IR laser irradiation times are <100 ms, and the laser power is maintained at 0.2 W across the entire tuning range. The laser bandwidth is 0.3−1 cm^{-1}, and the wavenumber step was set to 1.3 cm^{-1} in the present work.
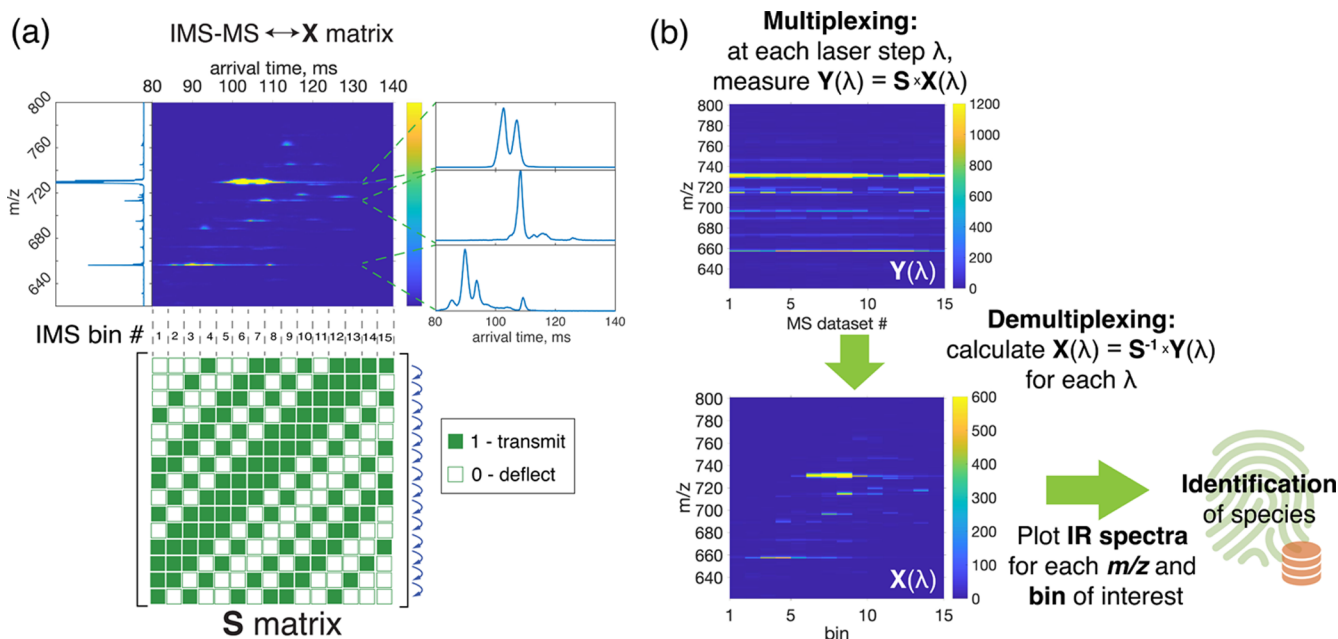

Figure 2. (a) Example of a relatively complex IMS−MS profile with multiple species separated using SLIM−IMS (human milk oligosaccharide mixture, total drift length 10 m). The IMS−MS profile can be split into N bins and represents the quantity of interest **X** upon multiplexing with the Simplex matrix **S** ($N \times N$). (b) Multiplexing and demultiplexing procedure, showing the example of multiplexed data **Y** = **S** × **X**, where **S** is a (15 × 15) Simplex matrix and **X** is the IMS−MS profile from panel (a).
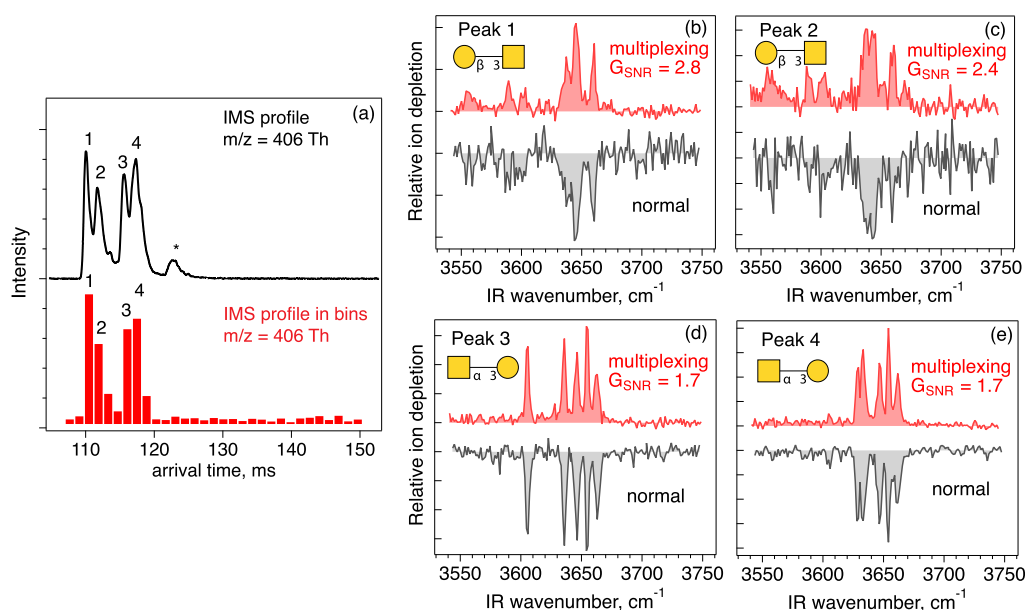
Figure 3. (a) ATD of a mixture of two disaccharides, GalNAc-α(1−3)-Gal and Gal-β(1−3)-GalNAc, in the [M + Na]$^+$ state, acquired after 12 SLIM-IMS separation cycles (18 m drift length) using the quadrupole mass filter and the channeltron detector, compared to the IMS profile recorded in 31 bins, 1.4 ms/bin using TOF−MS. The peak marked with the asterisk is due to an impurity that was not filtered by the quadrupole. (b−e) Cryogenic IR spectra of individual peaks separated by SLIM−IMS obtained using our multiplexed approach (red) compared with the spectra obtained under normal non-multiplexed measurements (gray). Multiplexed IR spectroscopy was performed using S(31 × 31) in the arrival time window of 107−150 ms, which was split into 31 bins of 1.4 ms duration. Non-multiplexed data were acquired directly after the multiplexed laser scan under the same experimental conditions and using the same width and the number of bins.

Arrival time distributions (ATDs) of ions following SLIM−IMS separation are obtained using a channeltron detector after m/z selection by the quadrupole mass filter. Alternatively, the two-dimensional IMS−MS profiles covering all m/z values of complex samples can be obtained by scanning a narrow transmission window (e.g., 300 μs) in the arrival time dimension and acquiring mass spectra corresponding to this window using TOF−MS.

Multiplexed Spectroscopy Approach. Multiplexed spectroscopy based on Hadamard transform measures the IR response of multiple known combinations of IMS peaks in a single laser scan and allows one to obtain the spectrum of individual IMS peaks with an increased SNR, a property known as the multiplex or Fellgett advantage.[45−48] In what follows, we describe the basics of the multiplexing approach applicable to cryogenic ion spectroscopy combined with IMS.

Initially, the IMS−MS profile of the sample is measured, and the window of interest covering all IMS peaks of interest is selected and split into N bins. Multiplexing is then performed using a Simplex matrix $\mathbf{S}(N \times N)$, which is a cyclic binary matrix derived from Hadamard matrices. The first row of $\mathbf{S}$ corresponds to a binary pseudorandom sequence of ones and zeros,[48] whereas the next rows correspond to a cyclic shift of the previous row one place to the left (see Figure 2a). We typically use N equal to 15, 19, 23, or 31 bins of width chosen such that two IMS peaks having the same m/z do not overlap in one bin. During multiplexed spectroscopy scans, the ions in the IMS bins that correspond to zeros in each row of the $\mathbf{S}$ matrix are deflected, whereas ions that correspond to ones are sent to the cryogenic trap, where they are cooled, tagged, irradiated with the IR laser, and mass analyzed using TOF−MS. We then decode this multiplexed IMS−MS data to obtain the mass spectra of individual IMS peaks at each laser wavelength λ, which in turn can be used to obtain their

messenger-tagging IR spectra as described above. The deflection of ions that correspond to zeros in the $\mathbf{S}$ matrix is performed by increasing the voltage on one of the elements of the ion steering lens (see Figure 1) and is controlled by the digital output module of a PCIe-6351 card (National Instruments) using a LabView program. Ion deflection in our setup allows producing rectangular-shaped pulses with rise and fall times of approximately 3 μs. Therefore, if required, the minimal bin length for multiplexing can be as short as ∼20 microseconds.

Mathematically, multiplexing implies that at each laser wavelength λ, we measure the encoded matrix $\mathbf{Y}(\lambda) = \mathbf{S} \times \mathbf{X}(\lambda)$, where $\mathbf{S}$ is an $(N \times N)$ Simplex matrix, $\mathbf{X}(\lambda)$ is an $(N \times k)$ matrix that contains the individual mass spectra of N bins in the selected ATD window (Figure 2a), and k is the length of the MS data vector. One may see that the measured $\mathbf{Y}(\lambda)$ matrices contain various known combinations of mass spectra of different IMS bins (Figure 2b). Upon data analysis, we multiply the $\mathbf{Y}(\lambda)$ matrices with the inverse of the $\mathbf{S}$ matrix to obtain the individual MS traces in each IMS bin [i.e., we compute $\mathbf{X}(\lambda) = \mathbf{S}^{-1} \times \mathbf{Y}(\lambda)$ at each λ]. This demultiplexing step is fast and can be performed while scanning the laser wavelength.

In this approach, the theoretical Fellgett advantage (i.e., the increase in the SNR using multiplexed spectroscopy compared to normal spectroscopy of single species) can be estimated as[47]

$$(G_{SNR})_i = \frac{SNR_{multiplexed}}{SNR_{normal}} = \left(\frac{x_i}{2\overline{x}}\right)^{1/2} \tag{1}$$

where x_i is the signal intensity of the m/z channel of interest in the ith IMS bin and $\overline{x}$ is defined as $\overline{x} = \frac{1}{N+1}\sum_{i=1}^{N} x_i$ which for high N is approximately equal to an average signal across all the IMS bins in the m/z channel of interest. Equation 1 is valid
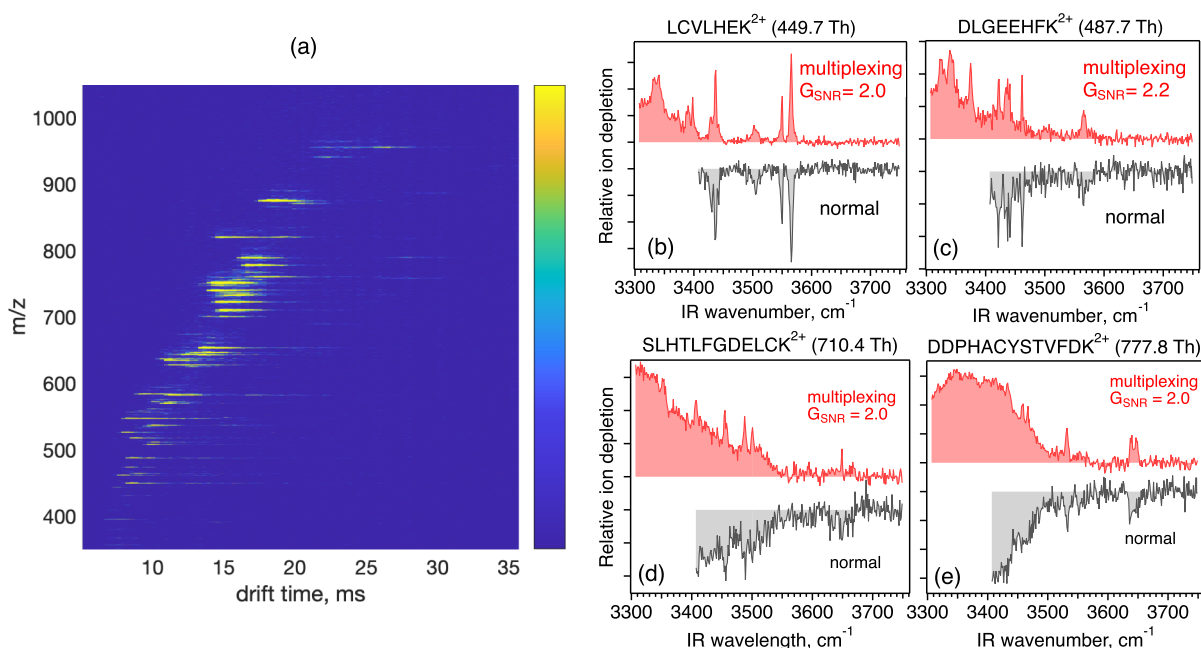
Figure 4. (a) IMS−MS profile acquired for the BSA protein digest sample after a single-cycle SLIM−IMS separation (drift length of 1.5 m). (b−e) Examples of peptide cryogenic IR spectra obtained using our multiplexed approach (red) compared with the spectra obtained using a normal, non-multiplexed approach (gray) under the same experimental conditions. Multiplexed IR spectroscopy was performed using $S(23 \times 23)$ in the arrival time window of 5−36 ms, which was split into 23 bins of 1.35 ms each. Normal (non-multiplexed) data were acquired directly after the multiplexed laser scan using the same arrival time window and number of bins.

for shot-noise limited conditions, which are intrinsic to TOF−MS measurements, and it implies that an increase in the SNR will be observed for all IMS bins with an intensity twice higher than the average intensity across all bins for the m/z value of interest. This is typically the case for sparce ATDs with just a few IMS peaks in each m/z channel, which we often obtain using ultrahigh-resolution SLIM−IMS separations of complex mixtures with a broad range of mobilities. Equation 1 also shows that the SNR of weak IMS peaks under the presence of strong peaks with the same m/z value will show a decrease in SNR upon multiplexing. Such weak IMS peaks can be identified at the initial stage of ATD inspection, and if necessary, they can be spectroscopically analyzed individually.

It is worth noting that Hadamard transform multiplexing was previously applied in ion mobility instruments in order to increase their duty cycle when coupled with continuous ion sources such as ESI.[49−53] In this case, multiplexing was achieved by sending multiple identical ion packets for separation by the IMS device in a single experimental cycle, which allowed increasing the SNR and resolution in the ion mobility dimension. We employ a drastically different approach, since our goal is to obtain IR spectra of ion packets that have different ion mobility.

Materials. Disaccharide GalNAc-α(1−3)-Gal was purchased from Dextra (UK), whereas Gal-β(1−3)-GalNAc and human milk oligosaccharide samples were purchased from Carbosynth (UK). Bovine serum albumin (BSA) protein digest was purchased from Thermo Fisher Scientific. All samples were used without further purification. For electrospray, the disaccharide samples were dissolved in water/methanol (v/v 50/50) to a final concentration of 5−50 μM, and the BSA protein digest was dissolved in water to yield a 0.5 μM concentration.

RESULTS AND DISCUSSION

We first demonstrate a multiplexed spectroscopy approach by analyzing a mixture of two isomeric disaccharides, GalNAc-α(1−3)-Gal and Gal-β(1−3)-GalNAc, which we separate after twelve SLIM−IMS roundtrips (total drift length of 18 m). The ATD corresponding to $[M + Na]^+$ ions (m/z 406) is shown in black in Figure 3a, where four major peaks can be observed. More specifically, each disaccharide exhibits two ion mobility peaks, which likely originate from reducing-end anomers, as was shown in our previous work.[35−37] For multiplexing, the ATD was split into 31 bins of 1.4 ms each, as shown in red in Figure 3a, and the IMS−MS data was encoded with an $S(31 \times 31)$ matrix at each laser wavelength step. The peaks of interest that represent the two disaccharides can be found within bins 3, 4, 7, and 8 (Figure 3a). The spectra corresponding to these bins are shown in Figures 3b−e and were obtained by demultiplexing the encoded IMS−MS data for each laser wavelength and plotting the ratio between the messenger-tagged and total ion signal of the disaccharide species.

Spectra in the free OH stretch region obtained in this way were compared to the reference spectra acquired using isomerically pure samples (Figure S1, Supporting Information), allowing us to assign peaks 1−2 to Gal-β(1−3)-GalNAc and peaks 3−4 to GalNAc-α(1−3)-Gal.

For the purpose of comparing the SNR of multiplexed and normal scans, the grey traces in Figure 3b−e show the corresponding laser scans acquired with the same settings but without multiplexing (i.e., S equals the identity matrix). One can see that the SNR improves upon multiplexing, allowing us to obtain high quality spectra in a shorter period of time. In order to estimate the SNR gain quantitively, we have analyzed the noise levels of multiplexed and non-multiplexed measurements by determining the standard deviation of data within the baseline of each spectrum where no depletion peaks occur

($3680-3750$ cm^{-1}). We find that the observed gain in SNR, G_{SNR}, reaches values between 1.7 and 2.8, depending on the IMS peak of interest (see Figure 3b−e), and agrees well with the theoretical estimation using eq 1. On average, an SNR increase of 2.14 is observed, and this corresponds to a reduction in analysis time by a factor of 4.6.

Next, we demonstrate the high-throughput nature of this multiplexed spectroscopy approach by analyzing a BSA protein digest mixture. Figure 4a shows the IMS−MS profile after a single-cycle separation using our compact SLIM−IMS device (1.5 m drift length). Even though in this case we do not separate peptide isomers or conformers, rapid separation by SLIM−IMS reduces the sample complexity for spectroscopic analysis. Indeed under cryogenic conditions (40 K), every peak visible in Figure 4a splits into several m/z channels due to the nitrogen tagging process, and SLIM−IMS separation helps to eliminate the possible crosstalk between the peptide IR spectra due to the overlapping m/z channels under the limited mass resolution of our TOF analyzer. Our multiplexed spectroscopy analysis covered the arrival time window of 5−36 ms (see Figure 4a) that was split into 23 bins of 1.35 ms each for multiplexing using $\mathbf{S}(23 \times 23)$. As a result, we have obtained high-quality cryogenic IR spectra of 37 peptide species in a single 24 min-long laser scan that covered the diagnostic frequency range of 3300−3700 cm^{-1}, probing vibrations corresponding to free and hydrogen-bonded OH/NH stretching. Figure 4b−e shows several examples of spectra obtained using multiplexing (red) compared to the non-multiplexed data (grey) obtained under identical experimental conditions (e.g., same arrival time window, bin width, and bin number). The comparison clearly indicates a significant improvement in the SNR thanks to the multiplex advantage. More specifically, we have obtained an average SNR gain across all species, $\langle G_{SNR} \rangle$, equal to 1.8 ± 0.2. This value is slightly lower than the estimated theoretical value of 2.1 ± 0.3 obtained using eq 1, possibly due to slightly decreased messenger-tagging efficiency upon multiplexing due to the presence of much larger ion populations in the cryogenic ion trap compared to non-multiplexed analysis. Nevertheless, the obtained SNR gain of 1.8 implies that without multiplexing one has to average data ~3 times longer in order to reach the same SNR. The comparison presented in Figure 4e also demonstrates that improved SNR can in some cases lead to a better resolved peak pattern, which can provide a more reliable identification of species based on their database spectra. These results clearly demonstrate the power of high-throughput multiplexed spectroscopy when spectra of all species in a complex mixture need to be acquired with high accuracy in a relatively short time.

CONCLUSIONS

In this work, we demonstrate a Hadamard transform multiplexing approach that allows measuring the IR spectra of all species present in a complex mixture in a single laser scan. This method is particularly promising for the analysis of complex mixtures with high isomeric complexity and can easily be implemented in various IMS−MS-spectroscopy setups. For example, in addition to its use in cryogenic IR spectroscopy employed in this work, the method can be used with IRMPD and UV spectroscopy. Moreover, one can use this method for multiplexed fragmentation of mobility selected species as well as for IMS^{n} analysis, which can provide alternative identification means for isomers.[38,43,54]

In the future, we plan to combine the presented multiplexed approach with significantly higher-resolution SLIM−IMS separations.[42,44] Furthermore, combining Hadamard transform with our cryogenic multi-trap approach[42] will significantly increase the throughput of spectroscopic analysis for unambiguous identification of molecular isomers in highly complex mixtures. This process can also be significantly accelerated by reducing the laser wavenumber range employed for isomer identification[42] using an algorithm that analyzes the reference spectra of candidate structures.

ASSOCIATED CONTENT

ⓢ Supporting Information

The Supporting Information is available free of charge at https://pubs.acs.org/doi/10.1021/acs.analchem.1c04843.

Comparison between the spectra obtained using multiplexing and the database spectra of disaccharide isomers (PDF)

AUTHOR INFORMATION

Corresponding Author

Vasyl Yatsyna − *Laboratoire de Chimie Physique Moléculaire, École Polytechnique Fédérale de Lausanne, EPFL SB ISIC LCPM, CH-1015 Lausanne, Switzerland; Department of Physics, University of Gothenburg, 412 96 Gothenburg, Sweden;* ⓞ orcid.org/0000-0002-3112-4298; Email: vasyl.yatsyna@epfl.ch

Authors

Ali H. Abikhodr − *Laboratoire de Chimie Physique Moléculaire, École Polytechnique Fédérale de Lausanne, EPFL SB ISIC LCPM, CH-1015 Lausanne, Switzerland;* ⓞ orcid.org/0000-0002-9235-0774

Ahmed Ben Faleh − *Laboratoire de Chimie Physique Moléculaire, École Polytechnique Fédérale de Lausanne, EPFL SB ISIC LCPM, CH-1015 Lausanne, Switzerland;* ⓞ orcid.org/0000-0002-9144-2052

Stephan Warnke − *Laboratoire de Chimie Physique Moléculaire, École Polytechnique Fédérale de Lausanne, EPFL SB ISIC LCPM, CH-1015 Lausanne, Switzerland;* ⓞ orcid.org/0000-0001-7481-286X

Thomas R. Rizzo − *Laboratoire de Chimie Physique Moléculaire, École Polytechnique Fédérale de Lausanne, EPFL SB ISIC LCPM, CH-1015 Lausanne, Switzerland;* ⓞ orcid.org/0000-0003-2796-905X

Complete contact information is available at:
https://pubs.acs.org/10.1021/acs.analchem.1c04843

Notes

The authors declare no competing financial interest.

REFERENCES

(1) Han, L.; Costello, C. E. *Biochem.* **2013**, *78*, 710−720.

(2) Reyes, C. D. G.; Jiang, P.; Donohoo, K.; Atashi, M.; Mechref, Y. S. *J. Sep. Sci.* **2021**, *44*, 403−425.

(3) Peng, W.; Reyes, C. D. G.; Gautam, S.; Yu, A.; Cho, B. G.; Goli, M.; Donohoo, K.; Mondello, S.; Kobeissy, F.; Mechref, Y. *Mass Spectrom. Rev.* **2021**, 1−40, DOI: 10.1002/mas.21713.

(4) Lu, W.; Su, X.; Klein, M. S.; Lewis, I. A.; Fiehn, O.; Rabinowitz, J. D. *Annu. Rev. Biochem.* **2017**, *86*, 277−304.

(5) Opialla, T.; Kempa, S.; Pietzke, M. *Metabolites* **2020**, *10*, 457.

(6) Harris, R. A.; Leaptrot, K. L.; May, J. C.; McLean, J. A. *TrAC, Trends Anal. Chem.* **2019**, *116*, 316−323.

(7) PortaSiegel, T. .; Ekroos, K. .; Ellis, S. .R. . *Angew. Chem., Int. Ed.* **2019**, *58*, 6492−6501.

(8) Mulloy, B.; Dell, A.; Stanley, P.; J, H. P. *Essentials of Glycobiology*; Varki, A.; Cummings, R. D.; Esko, J. D.; Stanley, P.; Hart, G. W.; Aebi, M.; Darvill, A. G.; Kinoshita, T.; Packer, N. H.; Prestegard, J. H.; Schnaar, R. L.; Seeberger, P. H., Eds.; Cold Spring Harbor (NY), 2015; pp 639−652.

(9) Smith, R. D.; Shen, Y.; Tang, K. *Acc. Chem. Res.* **2004**, *37*, 269−278.

(10) Nagy, G.; Peng, T.; Pohl, N. L. B. *Anal. Methods* **2017**, *9*, 3579−3593.

(11) Lu, G.; Crihfield, C. L.; Gattu, S.; Veltri, L. M.; Holland, L. A. *Chem. Rev.* **2018**, *118*, 7867−7885.

(12) Halket, J. M.; Waterman, D.; Przyborowska, A. M.; Patel, R. K. P.; Fraser, P. D.; Bramley, P. M. *J. Exp. Bot.* **2004**, *56*, 219−243.

(13) Delvaux, A.; Rathahao-Paris, E.; Alves, S. *Mass Spectrom. Rev.* **2021**, 1−27, DOI: 10.1002/mas.21685.

(14) Garcia, X.; Sabaté, M.; Aubets, J.; Jansat, J.; Sentellas, S. *Separations* **2021**, *8*, 33.

(15) Chen, Z.; Glover, M. S.; Li, L. *Curr. Opin. Chem. Biol.* **2018**, *42*, 1−8.

(16) Deng, L.; Ibrahim, Y. M.; Hamid, A. M.; Garimella, S. V. B.; Webb, I. K.; Zheng, X.; Prost, S. A.; Sandoval, J. A.; Norheim, R. V.; Anderson, G. A.; Tolmachev, A. V.; Baker, E. S.; Smith, R. D. *Anal. Chem.* **2016**, *88*, 8957−8964.

(17) Hamid, A. M.; Ibrahim, Y. M.; Garimella, S. V. B.; Webb, I. K.; Deng, L.; Chen, T.-C.; Anderson, G. A.; Prost, S. A.; Norheim, R. V.; Tolmachev, A. V.; Smith, R. D. *Anal. Chem.* **2015**, *87*, 11301−11308.

(18) Ujma, J.; Ropartz, D.; Giles, K.; Richardson, K.; Langridge, D.; Wildgoose, J.; Green, M.; Pringle, S. *J. Am. Soc. Mass Spectrom.* **2019**, *30*, 1028−1037.

(19) Causon, T. J.; Hann, S. *J. Am. Soc. Mass Spectrom.* **2020**, *31*, 2102−2110.

(20) Stow, S. M.; Causon, T. J.; Zheng, X.; Kurulugama, R. T.; Mairinger, T.; May, J. C.; Rennie, E. E.; Baker, E. S.; Smith, R. D.; McLean, J. A.; Hann, S.; Fjeldsted, J. C. *Anal. Chem.* **2017**, *89*, 9048−9055.

(21) Paglia, G.; Williams, J. P.; Menikarachchi, L.; Thompson, J. W.; Tyldesley-Worster, R.; Halldórsson, S.; Rolfsson, O.; Moseley, A.; Grant, D.; Langridge, J.; Palsson, B. O.; Astarita, G. *Anal. Chem.* **2014**, *86*, 3985−3993.

(22) Nichols, C. M.; Dodds, J. N.; Rose, B. S.; Picache, J. A.; Morris, C. B.; Codreanu, S. G.; May, J. C.; Sherrod, S. D.; McLean, J. A. *Anal. Chem.* **2018**, *90*, 14484−14492.

(23) Fouque, D. D. J.; Maroto, A.; Memboeuf, A. *Anal. Chem.* **2016**, *88*, 10821−10825.

(24) Ashline, D. J.; Zhang, H.; Reinhold, V. N. *Anal. Bioanal. Chem.* **2017**, *409*, 439−451.

(25) Liew, C. Y.; Yen, C.-C.; Chen, J.-L.; Tsai, S.-T.; Pawar, S.; Wu, C.-Y.; Ni, C.-K. *Commun. Chem.* **2021**, *4*, 92.

(26) Tan, Y.; Zhao, N.; Liu, J.; Li, P.; Stedwell, C. N.; Yu, L.; Polfer, N. C. *J. Am. Soc. Mass Spectrom.* **2017**, *28*, 539−550.

(27) Schindler, B.; Barnes, L.; Renois, G.; Gray, C.; Chambert, S.; Fort, S.; Flitsch, S.; Loison, C.; Allouche, A.-R.; Compagnon, I. *Nat. Commun.* **2017**, *8*, 973.

(28) Hernandez, O.; Isenberg, S.; Steinmetz, V.; Glish, G. L.; Maitre, P. *J. Phys. Chem. A* **2015**, *119*, 6057−6064.

(29) Martens, J.; van Outersterp, R. E.; Vreeken, R. J.; Cuyckens, F.; Coene, K. L. M.; Engelke, U. F.; Kluijtmans, L. A. J.; Wevers, R. A.; Buydens, L. M. C.; Redlich, B.; Berden, G.; Oomens, J. *Anal. Chim. Acta* **2020**, *1093*, 1−15.

(30) Martens, J.; Koppen, V.; Berden, G.; Cuyckens, F.; Oomens, J. *Anal. Chem.* **2017**, *89*, 4359−4362.

(31) Gorlova, O.; Colvin, S. M.; Brathwaite, A.; Menges, F. S.; Craig, S. M.; Miller, S. J.; Johnson, M. A. *J. Am. Soc. Mass Spectrom.* **2017**, *28*, 2414−2422.

(32) Mucha, E.; Flórez, A. I. G.; Marianski, M.; Thomas, D. A.; Hoffmann, W.; Struwe, W. B.; Hahm, H. S.; Gewinner, S.; Schöllkopf, W.; Seeberger, P. H.; von Helden, G.; Pagel, K. *Angew. Chem., Int. Ed.* **2017**, *56*, 11248−11251.

(33) Lettow, M.; Greis, K.; Grabarics, M.; Horlebein, J.; Miller, R. L.; Meijer, G.; von Helden, G.; Pagel, K. *J. Phys. Chem. A* **2021**, *125*, 4373−4379.

(34) Lettow, M.; Grabarics, M.; Greis, K.; Mucha, E.; Thomas, D. A.; Chopra, P.; Boons, G.-J.; Karlsson, R.; Turnbull, J. E.; Meijer, G.; Miller, R. L.; von Helden, G.; Pagel, K. *Anal. Chem.* **2020**, *92*, 10228−10232.

(35) Warnke, S.; Faleh, A. B.; Scutelnic, V.; Rizzo, T. R. *J. Am. Soc. Mass Spectrom.* **2019**, *30*, 2204−2211.

(36) Faleh, A. B.; Warnke, S.; Rizzo, T. R. *Anal. Chem.* **2019**, *91*, 4876−4882.

(37) Warnke, S.; Faleh, A. B.; Pellegrinelli, R. P.; Yalovenko, N.; Rizzo, T. R. *Faraday Discuss.* **2019**, *217*, 114−125.

(38) Pellegrinelli, R. P.; Yue, L.; Carrascosa, E.; Warnke, S.; Faleh, A. B.; Rizzo, T. R. *J. Am. Chem. Soc.* **2020**, *142*, 5948−5951.

(39) Dyukova, I.; Faleh, A. B.; Warnke, S.; Yalovenko, N.; Yatsyna, V.; Bansal, P.; Rizzo, T. R. *Analyst* **2021**, *146*, 4789−4795.

(40) Yalovenko, N.; Yatsyna, V.; Bansal, P.; AbiKhodr, A. H.; Rizzo, T. R. *Analyst* **2020**, *145*, 6493−6499.

(41) Khanal, N.; Masellis, C.; Kamrath, M. Z.; Clemmer, D. E.; Rizzo, T. R. *Anal. Chem.* **2017**, *89*, 7601−7606.

(42) Warnke, S.; Faleh, A. B.; Rizzo, T. R. *ACS Meas. Sci. Au* **2021**, *1*, 157−164.

(43) Bansal, P.; Yatsyna, V.; AbiKhodr, A. H.; Warnke, S.; Faleh, A. B.; Yalovenko, N.; Wysocki, V. H.; Rizzo, T. R. *Anal. Chem.* **2020**, *92*, 9079−9085.

(44) Deng, L.; Webb, I. K.; Garimella, S. V. B.; Hamid, A. M.; Zheng, X.; Norheim, R. V.; Prost, S. A.; Anderson, G. A.; Sandoval, J. A.; Baker, E. S.; Ibrahim, Y. M.; Smith, R. D. *Anal. Chem.* **2017**, *89*, 4628−4634.

(45) Zare, R. N.; Fernández, F. M.; Kimmel, J. R. *Angew. Chem., Int. Ed.* **2003**, *42*, 30−35.

(46) Brock, A.; Rodriguez, N.; Zare, R. N. *Anal. Chem.* **1998**, *70*, 3735−3741.

(47) Larson, N. M.; Crosmun, R.; Talmi, Y. *Appl. Opt.* **1974**, *13*, 2662−2668.

(48) Harwit, M.; Sloane, N. J. A. An Introduction to Optical Multiplexing Techniques. *Hadamard Transform Optics*; Harwit, M., Sloane, N. J. A., Eds.; Academic Press, 1979; pp 1−19.

(49) Clowers, B. H.; Siems, W. F.; Hill, H. H.; Massick, S. M. *Anal. Chem.* **2006**, *78*, 44−51.

(50) Belov, M. E.; Buschbach, M. A.; Prior, D. C.; Tang, K.; Smith, R. D. *Anal. Chem.* **2007**, *79*, 2451−2462.

(51) Ibrahim, Y. M.; Baker, E. S.; Danielson, W. F.; Norheim, R. V.; Prior, D. C.; Anderson, G. A.; Belov, M. E.; Smith, R. D. *Int. J. Mass Spectrom.* **2015**, *377*, 655−662.

(52) Clowers, B. H.; Cabrera, E.; Anderson, G.; Deng, L.; Moser, K.; Van Aken, G.; DeBord, J. D. *Anal. Chem.* **2021**, *93*, 5727−5734.

(53) Reinecke, T.; Naylor, C. N.; Clowers, B. H. *TrAC, Trends Anal. Chem.* **2019**, *116*, 340−345.

(54) Peterson, T. L.; Nagy, G. *Anal. Chem.* **2021**, *93*, 9397−9407.